

Learned Conjugate Gradient Descent Network for Massive MIMO Detection

Yi Wei, Ming-Min Zhao, Min-jian Zhao and Ming Lei

Abstract—In this work, we consider the use of model-driven deep learning techniques for massive multiple-input multiple-output (MIMO) detection. Compared with conventional MIMO systems, massive MIMO promises improved spectral efficiency, coverage and range. Unfortunately, these benefits are coming at the cost of significantly increased computational complexity. To reduce the complexity of signal detection and guarantee the performance, we present a learned conjugate gradient descent network (LcgNet), which is constructed by unfolding the iterative conjugate gradient descent (CG) detector. In the proposed network, instead of calculating the exact values of the scalar step-sizes, we explicitly learn their universal values. Also, we can enhance the proposed network by augmenting the dimensions of these step-sizes. Furthermore, in order to reduce the memory costs, a novel quantized LcgNet is proposed, where a low-resolution nonuniform quantizer is used to quantize the learned parameters. The quantizer is based on a specially designed soft staircase function with learnable parameters to adjust its shape. Meanwhile, due to fact that the number of learnable parameters is limited, the proposed networks are easy and fast to train. Numerical results demonstrate that the proposed network can achieve promising performance with much lower complexity.

Index Terms—Conjugate gradient descent, deep learning, massive MIMO detection, model-driven method.

I. INTRODUCTION

Massive multiple-input multiple-output (MIMO), which has attracted much attention from both academia and industry, is a promising technology to potentially achieve higher spectral efficiency over existing (small-scale) MIMO systems [1], [2]. The main idea of massive MIMO is to equip the transmitter or receiver with a large number of antennas, however this also brings unbearable pressure to signal detection in terms of computational complexity. Therefore, efficient massive MIMO detection algorithms with low complexity and good bit error rate (BER) performance play important roles in the receiver design.

A. Literature Review on Massive MIMO Detection

Generally, the maximum likelihood (ML) detector is considered to be optimal, but it requires an exhaustive search on all the combinations of transmit symbols, which exhibits exponential computational complexity. Therefore, near-optimal algorithms are usually preferred, e.g., the approximate message passing (AMP) detector [3], the semidefinite relaxation (SDR) detector [4], [5], etc. Fortunately, besides higher peak data rates, enhanced link reliability, and improved coverage, theoretical results also indicate that simple, low-complexity and energy-efficient detection algorithms exist

when the number of antennas approaches infinity [6], [7]. Some linear detectors, such as the zero forcing (ZF) detector and the minimum mean squared error (MMSE) detector, have been proved to be near-optimal for massive MIMO systems [1]. However, they still require the complex matrix inversion operation. To further reduce the computational complexity, detectors based on truncated Neumann series expansion were proposed in [8]–[10], where the matrix inversion operation is transformed into a series of matrix-vector multiplications. In [11]–[13], the conjugate gradient descent (CG) algorithm was employed to iteratively achieve the performance of the MMSE detector with lower complexity. It was shown in [11] that the CG detector outperforms those based on truncated Neumann series expansions in terms of both BER performance and computational complexity. Except for the ML detector, few works were reported in the literature to outperform the MMSE detector for large scale MIMO systems.

B. Background on Deep Learning

As a popular approach to artificial intelligence, deep learning (DL) has revolutionized many fields, e.g., computer vision and natural language processing, and it has been widely applied to solve wireless physical layer communication problems recently [14]. DL based methods can be grossly divided into two subcategories: 1) data-driven methods, which treat the network as a black box and train it by a huge volume of data, e.g., deep neural networks (DNNs) for channel encoding/decoding [15], channel estimation [16], modulation recognition [17] and channel state information (CSI) feedback [18], etc., 2) model-driven methods, which are constructed based on known domain knowledge and physical mechanism, such as the Lam-ResNet for mmWave channel estimation [19] and the OFDM-autoencoder [20]. In particular, in order to construct a network, model-driven DL methods usually unfold a existing iterative algorithm, add some adjustable parameters and then train these parameters by DL. For instance, in [21] and [22], the AMP and iterative thresholding (ISTA) algorithms were improved by unfolding their iterations into networks and learning the corresponding parameters.

Given the promising advantages of model-driven DL methods, they have also been applied to MIMO detection recently [23]–[27]. Specifically, the detection network (DetNet) was proposed in [23] by mimicking a projected gradient descent (PG) like solution for the maximum likelihood optimization. It was shown in [23] that DetNet achieves a comparable performance to those of the SDR and AMP detectors but with less detecting time. This performance improvement was achieved at the expense of high computational complexity in the offline training process, which took about three days on a

Y. Wei, M. M. Zhao, M. J. Zhao and M. Lei are with College of Information Science and Electronic Engineering, Zhejiang University, Hangzhou 310027, China (email: {21731133, zmmblack, mjzhao, lm1029}@zju.edu.cn)

standard Intel i7-6700 processor. The works [24] and [25] also applied this idea to massive overloaded MIMO detection and multi-level MIMO detection, respectively, and comparable detection performance to those of the state-of-the-art algorithms was achieved. In [26] and [27], DL based MIMO detection networks were proposed by unfolding the orthogonal AMP (OAMP) and belief propagation (BP) algorithms, respectively, and they were also demonstrated to significantly outperform the original algorithms by learning the parameters from a large number of training data.

C. Motivation and Contributions

In this work, inspired by model-driven DL method, we propose a CG based DL network structure, namely learned CG network (LcgNet), for massive MIMO detection. The proposed network is constructed by unfolding the iterations of the CG algorithm, and each layer can be viewed as one iteration with some additional adjustable parameters. By following the prototype of LcgNet, two variants are proposed with scalar and vector network parameters, which are referred to as LcgNetS and LcgNetV, respectively. Furthermore, in order to reduce the memory costs brought up by the storage of the step-sizes, we present a novel quantized LcgNetV (QLcgNetV), where the step-sizes are smartly quantized by carefully designing a low-resolution nonuniform quantizer.

The main contributions of this work can be summarized as follows:

1) In the proposed LcgNet, we treat the step-sizes of the CG detector as learnable (scalar and vector) parameters. We show that the performance of LcgNetS is almost identical to that of the CG/MMSE detector. Since the calculations of the step-sizes are simplified to some prestored parameters, the complexity of LcgNetS is much lower. Furthermore, significant performance gains over the CG/MMSE detector and other state-of-the-art detectors can be achieved by LcgNetV under both independent Rayleigh and correlated MIMO channels. The computational complexities of LcgNetV and LcgNetS are the same, but LcgNetV needs more memory space since more parameters are required to be stored.

2) A novel QLcgNetV is proposed to save the memory costs resulted from the storage of the vector step-sizes. In QLcgNetV, a new nonuniform quantizer is employed and it is jointly optimized with LcgNetV to compress the network parameters. This quantizer is based on a specially designed soft staircase function, also referred to as the *TanhSum* function, which consists of a series of Tanh functions. It is differentiable and has non-zero gradients everywhere. This appealing property allows us to integrate the proposed quantizer into the proposed network structure so that efficient training can be performed by backpropagation. We show that QLcgNetV can effectively reduce the memory costs, at the cost of some minor detection performance loss.

3) Due to the fact that the number of learnable parameters in the proposed networks is very limited compared with some commonly known network structures, such as the fully-connected DNNs, our training process is relatively simple and easy to implement. All the training is carried out offline, i.e.

once trained, the proposed networks can be used to detect the transmit signal online through one forward pass.

In order to promote reproducible research, the Python codes for generating most of the results in this work will be available on github once we have properly organized the codes.

D. Organization of the Paper and Notations

The rest of this paper is organized as follows. Section II presents the system model and formulates the massive MIMO detection problem. Next, we introduce the main idea of the CG detector and present the proposed LcgNet in Section III. Section IV provides the details of the proposed QLcgNetV. Numerical results are presented in Section V. Section VI concludes the paper. Finally, potential applications of our proposed LcgNet and some promising future research directions are given in Section VII.

Notation: Scalars, vectors and matrices are respectively denoted by lower (upper) case, boldface lower case and boldface upper case letters. x_n denotes the n -th entry of the vector \mathbf{x} . $\Re(\cdot)$ and $\Im(\cdot)$ denote the real and imaginary parts of their arguments respectively; $\|\cdot\|$, $E[\cdot]$, $|\cdot|$, $(\cdot)^{-1}$ and $(\cdot)^H$ denote the L2 norm, expectation, absolute, matrix inversion and conjugate transpose operations, respectively; $\mathbb{C}^{m \times n}$ ($\mathbb{R}^{m \times n}$) denotes the space of $m \times n$ complex (real) matrices, and \mathbb{R}^+ denotes the space of positive real numbers. The symbol \odot represents the hadamard product. We define the complex normal distribution as $\mathcal{CN}(\mu, \sigma^2)$ with mean μ and variance σ^2 . Finally, $\text{sgn}(\cdot)$ is used to denote the signum function, where $\text{sgn}(x) = 1$ when $x \geq 0$, and $\text{sgn}(x) = -1$ otherwise.

II. PRELIMINARIES ON MIMO DETECTION

A. System Model

We consider a massive MIMO system with N_t transmit antennas and N_r receive antennas, where $N_t \leq N_r$. Let $\mathbf{s} \in \mathbb{A}^{N_t \times 1}$ denote the unknown transmit signal vector, where \mathbb{A} is the modulation alphabet in the complex valued constellations, and let $\mathbf{H} \in \mathbb{C}^{N_r \times N_t}$ denote the complex channel matrix. Then, the received signal vector $\mathbf{y} \in \mathbb{C}^{N_r \times 1}$ can be written as

$$\mathbf{y} = \mathbf{H}\mathbf{s} + \mathbf{n}, \quad (1)$$

where $\mathbf{n} \sim \mathcal{CN}(0, \sigma_n^2 \mathbf{I}_{N_r})$ is the additive white Gaussian noise (AWGN).

To facilitate the process of DL, we avoid the handling of complex valued variables by employing an equivalent real-valued representation which is obtained by considering the real and imaginary parts separately. As a result, Eq. (1) can be rewritten as follows:

$$\mathbf{y}_r = \mathbf{H}_r \mathbf{s}_r + \mathbf{n}_r, \quad (2)$$

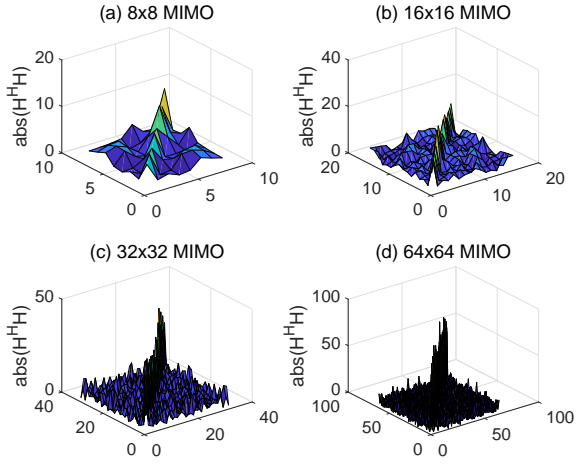


Fig. 1: An illustration of the channel hardening phenomenon.

where

$$\begin{aligned} \mathbf{y}_r &= \begin{bmatrix} \Re(\mathbf{y}) \\ \Im(\mathbf{y}) \end{bmatrix} \in \mathbb{R}^{2N_r \times 1}, \mathbf{s}_r = \begin{bmatrix} \Re(\mathbf{s}) \\ \Im(\mathbf{s}) \end{bmatrix} \in \mathbb{R}^{2N_t \times 1}, \\ \mathbf{n}_r &= \begin{bmatrix} \Re(\mathbf{n}) \\ \Im(\mathbf{n}) \end{bmatrix} \in \mathbb{R}^{2N_r \times 1}, \\ \mathbf{H}_r &= \begin{bmatrix} \Re(\mathbf{H}) & -\Im(\mathbf{H}) \\ \Im(\mathbf{H}) & \Re(\mathbf{H}) \end{bmatrix} \in \mathbb{R}^{2N_r \times 2N_t}. \end{aligned} \quad (3)$$

B. Massive MIMO Detection

The ML detector can achieve the optimal detection performance, measured by the minimum joint probability of error for detecting all the symbols simultaneously, however its computational complexity is exponential in N_t , which is prohibitive when the number of antennas is large. Fortunately, the channel-hardening phenomenon in massive MIMO system offers new opportunities for signal detection. As shown by the Marcenko-Pastur law [28], the singular values of \mathbf{H} become less sensitive to the actual distributions of its i.i.d. entries and the diagonal entries of $\mathbf{H}^H \mathbf{H}$ will become increasingly larger in magnitude than the off-diagonal ones as the size of \mathbf{H} increases. In other words, the channel becomes more and more deterministic with the increased number of antennas. As shown in Fig. 1, with the growth of the size of $\mathbf{H}^H \mathbf{H}$, the magnitudes of its diagonal entries converge to its dimension while the off-diagonal ones converge to 0. With channel-hardening, simple linear detection algorithms are able to achieve good performance in massive MIMO systems, such as the ZF and MMSE detectors. The main idea of these linear detectors is to obtain a preliminary estimation $\hat{\mathbf{s}}$ of the transmit symbol \mathbf{s} by multiplying \mathbf{y} with a receive filter \mathbf{G} , and then make decisions by mapping each element of $\hat{\mathbf{s}}$ into \mathbb{A} according to the minimum distance criterion. The ZF and MMSE detectors can be expressed as follows:

$$\hat{\mathbf{s}}_{\text{ZF}} = \mathbf{G}_{\text{ZF}} \mathbf{y} = (\mathbf{H}^H \mathbf{H})^{-1} \mathbf{H}^H \mathbf{y}, \quad (4)$$

$$\hat{\mathbf{s}}_{\text{MMSE}} = \mathbf{G}_{\text{MMSE}} \mathbf{y} = (\mathbf{H}^H \mathbf{H} + \sigma_n^2 \mathbf{I}_{N_t})^{-1} \mathbf{H}^H \mathbf{y}, \quad (5)$$

where \mathbf{I}_{N_t} represents an $N_t \times N_t$ identity matrix. Compared with the ZF detector, the MMSE detector takes the noise

into consideration and therefore results in an improved performance. As can be seen from Eq. (4) and Eq. (5), both ZF and MMSE detectors involve a matrix inversion operation. Since the dimension of the channel matrix in massive MIMO systems can be very large, their computational complexities will be considerable high.

III. LEARNED CG NETWORK

In this section, we first review the CG algorithm for linear MMSE detection [11]–[13], which is referred to as the CG detector in the following. It can iteratively achieve the performance of the MMSE detector without matrix inversion. Then, we present a detailed description of the proposed LcgNet and explain the intuition behind it. Finally, we provide the training strategy and complexity analysis of the proposed LcgNet.

A. The CG Detector

Let us rewrite the MMSE detector as follows:

$$\begin{aligned} \hat{\mathbf{s}}_{\text{MMSE}} &= (\mathbf{H}^H \mathbf{H} + \sigma_n^2 \mathbf{I}_{N_t})^{-1} \mathbf{H}^H \mathbf{y} \\ &= \mathbf{A}_{\text{MMSE}}^{-1} \mathbf{b}_{\text{MMSE}}, \end{aligned} \quad (6)$$

where $\mathbf{A}_{\text{MMSE}} = \mathbf{H}^H \mathbf{H} + \sigma_n^2 \mathbf{I}_{N_t}$ and $\mathbf{b}_{\text{MMSE}} = \mathbf{H}^H \mathbf{y}$ denote the Hermitian positive definite MMSE filtering matrix and matched-filter output vector, respectively. It can be seen that $\hat{\mathbf{s}}_{\text{MMSE}}$ can be viewed as the solution of the linear equation $\mathbf{A}_{\text{MMSE}} \mathbf{s} = \mathbf{b}_{\text{MMSE}}$.

CG is an efficient iterative algorithm to solve this linear equation with low computational consumption. For ease of notation, the aforementioned linear equation can be generally rewritten as

$$\mathbf{A} \mathbf{s} = \mathbf{b}, \quad (7)$$

where $\mathbf{A} \in \mathbb{C}^{K \times K}$ is a Hermitian positive definite matrix, $\mathbf{s} \in \mathbb{C}^{K \times 1}$ is the solution vector, and $\mathbf{b} \in \mathbb{C}^{K \times 1}$ is the measurement vector. Eq. (7) can be equivalently transformed into the following quadratic optimization problem:

$$\min_{\mathbf{s}} f(\mathbf{s}) \triangleq \left(\frac{1}{2} \mathbf{s}^T \mathbf{A} \mathbf{s} - \mathbf{b}^T \mathbf{s} \right). \quad (8)$$

Since \mathbf{A} is symmetric and positive definite, the gradient of $f(\mathbf{s})$ at the optimal point $\hat{\mathbf{s}}$ would be zero, i.e., $f'(\hat{\mathbf{s}}) = \mathbf{A} \hat{\mathbf{s}} - \mathbf{b} = \mathbf{0}$. Let $\mathcal{D} \triangleq \{\mathbf{d}^{(0)}, \mathbf{d}^{(1)}, \dots, \mathbf{d}^{(K-1)}\}$ denote the conjugate direction set with respect to \mathbf{A} , i.e., $(\mathbf{d}^{(i)})^H \mathbf{A} \mathbf{d}^{(j)} = 0, \forall i \neq j$. Then, we can minimize $f(\mathbf{s})$ in K steps by successively minimizing it along K individual conjugate directions in \mathcal{D} . By resorting to these conjugate directions, the

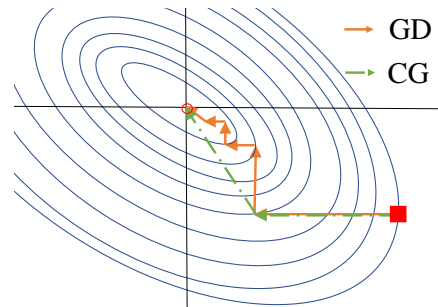


Fig. 2: The search procedures of the CG and GD algorithms.

Algorithm 1 The CG detector

Input: \mathbf{A} and \mathbf{b}
Output: Estimated transmit signal $\hat{\mathbf{s}}$

- 1: Initialization: $i = 0$, $\hat{\mathbf{s}}^{(0)} = \mathbf{0}$, $\hat{\mathbf{r}}^{(0)} = \mathbf{b}$, $\hat{\mathbf{d}}^{(0)} = \hat{\mathbf{r}}^{(0)}$.
 - 2: **while** $\hat{\mathbf{r}}^{(i)} \neq \mathbf{0}$ **do**
 - 3: Update $\alpha^{(i)}$ according to Eq. (12),
 - 4: Update $\hat{\mathbf{s}}^{(i+1)}$ according to Eq. (9),
 - 5: Update $\mathbf{r}^{(i+1)}$ according to Eq. (10),
 - 6: Update $\beta^{(i)}$ according to Eq. (13),
 - 7: Update $\hat{\mathbf{d}}^{(i+1)}$ according to Eq. (11),
 - 8: $i = i + 1$.
 - 9: **end while**
 - 10: **return** $\hat{\mathbf{s}} = \hat{\mathbf{s}}^{(i+1)}$.
-

CG algorithm usually exhibit faster convergence speed than conventional gradient descent algorithms, such as the steepest gradient descent algorithm (GD) [29]. The iterations of CG can be described as

$$\hat{\mathbf{s}}^{(i+1)} = \hat{\mathbf{s}}^{(i)} + \alpha^{(i)} \mathbf{d}^{(i)}, i = 0, 1, 2, \dots, \quad (9)$$

where i denotes the iteration index, and $\alpha^{(i)}$ is a scalar parameter which represents the step-size along direction $\mathbf{d}^{(i)}$. Furthermore, the residual $\mathbf{r}^{(i)}$ of the linear system (7), which is also the descent direction of GD for $f(\hat{\mathbf{s}}^{(i)})$, equals the negative gradient $-f'(\hat{\mathbf{s}}^{(i)})$, i.e.,

$$\mathbf{r}^{(i)} = -f'(\hat{\mathbf{s}}^{(i)}) = \mathbf{r}^{(i-1)} - \alpha^{(i-1)} \mathbf{A} \mathbf{d}^{(i-1)}. \quad (10)$$

In the CG algorithm, each direction $\mathbf{d}^{(i)}$ is selected as a linear combination of the previous direction $\mathbf{d}^{(i-1)}$ and the negative gradient $\mathbf{r}^{(i)}$, i.e.,

$$\mathbf{d}^{(i)} = \mathbf{r}^{(i)} + \beta^{(i-1)} \mathbf{d}^{(i-1)}, \quad (11)$$

where $\beta^{(i-1)}$ is a scalar parameter, serving as the step-size to update $\mathbf{d}^{(i)}$, and $\mathbf{d}^{(0)}$ is initialized as $\mathbf{r}^{(0)}$.

Fig. 2 illustrates the search procedures of the CG and GD algorithms, where the ellipses denote the level faces of $f(\mathbf{s})$, the solid orange and dashed green arrows depict the descent directions of GD ($\mathbf{r}^{(i)}$) and CG ($\mathbf{d}^{(i)}$), respectively. It can be observed that the search procedure of CG is not in zigzag shape, which shows that CG can achieve convergence with less iterations as compared with GD.

In addition, according to [29], the step-sizes $\alpha^{(i)}$ and $\beta^{(i)}$ can be exactly calculated as follows:

$$\alpha^{(i)} = \frac{(\mathbf{r}^{(i)})^H \mathbf{r}^{(i)}}{(\mathbf{r}^{(i)})^H \mathbf{A} \mathbf{d}^{(i)}}, \quad (12)$$

$$\beta^{(i)} = \frac{(\mathbf{r}^{(i+1)})^H \mathbf{r}^{(i+1)}}{(\mathbf{r}^{(i)})^H \mathbf{r}^{(i)}}. \quad (13)$$

To summarize, the CG detector [12] is listed in Algorithm 1.

B. The Proposed LcgNet

As one of the most popular and powerful schemes to build a model-driven DL network, simply unrolling a well-understood iterative algorithm is shown to outperform the baseline algorithm in many cases, such as the DetNet [23]

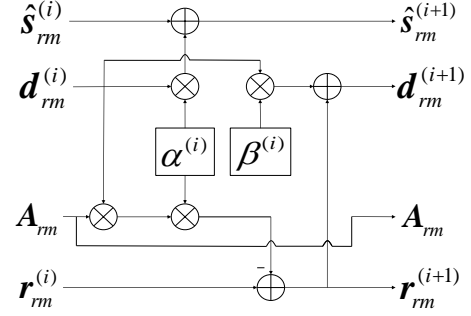


Fig. 3: The i -th layer of LcgNet with learnable parameters $\{\alpha_r^{(i)}, \beta_r^{(i)}\}$.

and the deep ADMM-net [30]. Inspired by this instructive idea, we design our LcgNet by unfolding the iterations of Algorithm 1 and transforming the step-sizes of each iteration into layer-dependent learnable parameters. The dimensions of the step-sizes can be augmented from scalars to vectors to further improve the detection performance. Compared with the CG detector, the proposed network can achieve better detection accuracy with lower computational complexity.

Let $\{(\mathbf{y}_{rm}, \mathbf{s}_{rm})\}_{m=1}^M$ denote the set of training samples with size M , where \mathbf{y}_{rm} and \mathbf{s}_{rm} are the m -th feature and label, respectively. Then, the proposed network is expected to accept \mathbf{y}_r as input and predict the label \mathbf{s}_r that corresponds to this \mathbf{y}_r . Our deep LcgNet is defined over a data flow graph based on the CG detector, which is shown in Fig. 3. The nodes in the graph correspond to different operations in CG, and the directed edges represent the data flows between these operations. The i -th iteration of the CG detector corresponds to the i -th stage/layer of LcgNet. Compared with the CG detector, whose step-sizes $\alpha^{(i)}$ and $\beta^{(i)}$ are calculated by (12) and (13) in the i -th iteration, we propose to introduce layer-dependent parameters $\Theta^{(i)} = \{\alpha_r^{(i)}, \beta_r^{(i)}\}$ into the i -th layer of LcgNet and learn these step-sizes from the training samples $\{(\mathbf{y}_{rm}, \mathbf{s}_{rm})\}_{m=1}^M$ by minimizing the following mean square error (MSE) loss function:

$$\begin{aligned} \mathcal{L}^{(L)}(\Theta^{(1)}, \dots, \Theta^{(L)}) \\ = \frac{1}{M} \sum_{m=1}^M \|\mathbf{s}_{rm} - \hat{\mathbf{s}}_r^{(L)}(\mathbf{y}_{rm}; \Theta^{(1)}, \dots, \Theta^{(L)})\|^2. \end{aligned} \quad (14)$$

In (14), L denotes the number of layers, and $\hat{\mathbf{s}}_r^{(L)}(\mathbf{y}_{rm}; \Theta^{(1)}, \dots, \Theta^{(L)})$ is the output of LcgNet with \mathbf{y}_{rm} as inputs and $\{\Theta^{(1)}, \dots, \Theta^{(L)}\}$ as parameters. As illustrated in Fig. 3, the i -th layer of LcgNet can be represented by

$$\hat{\mathbf{s}}_{rm}^{(i+1)} = \hat{\mathbf{s}}_{rm}^{(i)} + \alpha_r^{(i)} \mathbf{d}_{rm}^{(i)}, \quad (15a)$$

$$\mathbf{r}_{rm}^{(i+1)} = \mathbf{r}_{rm}^{(i)} - \alpha_r^{(i)} \mathbf{A}_{rm} \mathbf{d}_{rm}^{(i)}, \quad (15b)$$

$$\mathbf{d}_{rm}^{(i+1)} = \mathbf{r}_{rm}^{(i+1)} + \beta_r^{(i)} \mathbf{d}_{rm}^{(i)}, \quad (15c)$$

where $\hat{\mathbf{s}}_{rm}^{(0)} = \mathbf{0}$, $\mathbf{r}_{rm}^{(0)} = \mathbf{b}_{rm}$ and $\mathbf{d}_{rm}^{(0)} = \mathbf{r}_{rm}^{(0)}$ denote the first-layer inputs, $\mathbf{A}_{rm} = \mathbf{H}_{rm}^T \mathbf{H}_{rm} + \sigma_n^2 \mathbf{I}_{2N_t}$ and $\mathbf{b}_{rm} = \mathbf{H}_{rm}^T \mathbf{y}_{rm}$. It can be seen that in LcgNet, the calculations of $\alpha_r^{(i)}$ and $\beta_r^{(i)}$, which originally involve matrix-vector multiplication and division operations, are replaced by some prestored parameters which are fixed during online detections. Note that this can effectively reduce the computational complexities, only at the expense of some additional memory costs.

Moreover, we can further improve the performance of

LcgNet by lifting the scalar parameter $\Theta^{(i)}$ to a higher dimension, e.g., using vector step-sizes $\Theta_v^{(i)} = \{\alpha_r^{(i)} \in \mathbb{R}^{2N_t \times 1}, \beta_r^{(i)} \in \mathbb{R}^{2N_t \times 1}\}^1$. By following this idea, we are able to learn the appropriate values of these high dimensional step-sizes and this may have the potential to even outperform the original CG detector. For clarity, we refer the networks with scalar and vector step-sizes as LcgNetS and LcgNetV, respectively. For LcgNetV, similar to (17), the operations involved in the i -th layer can be expressed as

$$\hat{\mathbf{s}}_{rm}^{(i+1)} = \hat{\mathbf{s}}_{rm}^{(i)} + \alpha_r^{(i)} \odot \mathbf{d}_{rm}^{(i)}, \quad (16a)$$

$$\mathbf{r}_{rm}^{(i+1)} = \mathbf{r}_{rm}^{(i)} - \alpha_r^{(i)} \odot \mathbf{A}_{rm} \mathbf{d}_{rm}^{(i)}, \quad (16b)$$

$$\mathbf{d}_{rm}^{(i+1)} = \mathbf{r}_{rm}^{(i+1)} + \beta_r^{(i)} \odot \mathbf{d}_{rm}^{(i)}. \quad (16c)$$

Note that the computational complexity of (16) is almost identical to that of (17) in LcgNetS, however, in this case, more parameters are needed to be stored.

C. The Intuition behind the Proposed LcgNetV

In this subsection, we give the main motivation behind the proposed LcgNetV, which intuitively explain the reason why such an approach works.

For the sake of notation simplicity, we consider a K -dimensional vector space \mathcal{V} . Initialized at $\hat{\mathbf{s}}^{(0)}$, any gradient descent-type algorithms choose a direction $\mathbf{d}^{(i)}$ and then search along this direction with a proper step-size $\sigma^{(i)}$ for a new iteration in order to achieve a smaller distance to the optimal solution \mathbf{s}^* . Suppose that we can find the optimal solution after I iterations, i.e.,

$$\mathbf{s}^* = \hat{\mathbf{s}}^{(0)} + \sigma^{(0)} \mathbf{d}^{(0)} + \dots + \sigma^{(I-1)} \mathbf{d}^{(I-1)}. \quad (17)$$

One can view the above expression as gradient descent trying to find a set of vectors and the corresponding weights (step-sizes) whose weighted linear combination is equivalent to $\mathbf{s}^* - \hat{\mathbf{s}}^{(0)}$. Note that an arbitrary vector in space \mathcal{V} can be expressed as a linear combination of the basis vectors, and any set of K linearly independent vectors in \mathcal{V} is automatically a basis for this space.

The CG algorithm tries to find a set of conjugate directions, which are mutually independent [29], such that the number of iterations can be restricted to the space dimension, i.e., $I = K$. In our LcgNetV, (17) is transformed into

$$\mathbf{s}^* - \hat{\mathbf{s}}^{(0)} = \sigma^{(0)} \odot \mathbf{d}^{(0)} + \dots + \sigma^{(I-1)} \odot \mathbf{d}^{(I-1)}, \quad (18)$$

where the step-sizes $\{\sigma^{(i)}\}_{i=0}^{I-1}$ are in vector form. Consider a single problem instance, it can be readily seen

¹We have also investigated the case where matrix step-sizes are employed, however, only minor performance gain is observed. Therefore, in this work, we only consider the use of vector step-sizes.

that with a given $\mathbf{s}^* = [s_1^*, s_2^*, \dots, s_K^*]^T$ and a pre-chosen $\mathbf{d}^{(0)} = [d_1^{(0)}, d_2^{(0)}, \dots, d_K^{(0)}]^T$, where $\{d_j^{(0)}\}_{j=1}^K \neq 0$, we can always find a vector step-size $\sigma^{(0)} = [s_1^*/d_1^{(0)}, s_2^*/d_2^{(0)}, \dots, s_K^*/d_K^{(0)}]^T$ such that Eq. (18) can be satisfied. Therefore, by resorting to the power of DL, LcgNetV is expected to learn these high-dimensional parameters that can be applied to multiple scenarios with arbitrary \mathbf{s}^* . Simulation results corroborates that LcgNetV can indeed reduce the number of iterations and outperform the conventional CG detector, which will be elaborated in Section V.

D. Training Details

The proposed networks are implemented in Python using the TensorFlow library with the Adam optimizer [31].

Training/testing data: Since the proposed networks are expected to work at various signal-to-noise ratio (SNR) levels, we construct the training data set by randomly generating the training samples $\{(\mathbf{y}_{rm}, \mathbf{s}_{rm})\}_{m=1}^M$ based on (1) with different levels of channel noise. The transmit symbols in \mathbf{s} are from BPSK modulation and \mathbf{H} is randomly generated according to some specific channel model. The training and testing data sets contain 10^5 and 10^4 samples, respectively.

Training process: We first train the proposed networks using training samples with high SNR, e.g., SNR = 30 dB, in order to learn the intrinsic structure of the detection problem. Then, we employ the samples with lower SNRs in the subsequent training process for the purpose of reducing the influence caused by noise. More specifically, in order to gradually improve the robustness of the proposed networks against channel noise, the SNR levels of the training samples are chosen from the range [25, 20, 15, 10, 5, 0] dB successively. From the beginning, the step-sizes Θ and Θ_v are initialized as zeros. For each SNR level, we train the proposed network with the same strategy, which is described in details as follows.

The step-sizes Θ and Θ_v are trained by beginning with a single-layer network and then gradually increasing the network size one layer at a time. More specifically, when training the LcgNetS (LcgNetV) with l layers, we first train the parameters $\{\alpha_r^{(l)}, \beta_r^{(l)}\}$ ($\{\alpha_r^{(l)}, \beta_r^{(l)}\}$) in the current layer with $\{\alpha_r^{(i)}, \beta_r^{(i)}\}_{i=1}^{l-1}$ ($\{\alpha_r^{(i)}, \beta_r^{(i)}\}_{i=1}^{l-1}$) fixed, and the learning rate is set to be 0.001. After that, we finetune all the parameters $\{\alpha_r^{(i)}, \beta_r^{(i)}\}_{i=1}^l$ ($\{\alpha_r^{(i)}, \beta_r^{(i)}\}_{i=1}^l$) by using a decaying learning rate which is set to be 0.0005 initially and then reduce it by half in every epoch. All these training processes are terminated when the average validation normalized MSE (NMSE) stops decreasing. For clarity, we illustrate the training process of a 3-layer LcgNetV in Fig. 4 as a toy example, where the SNR levels of the training samples are chosen from [30, 10] dB successively.

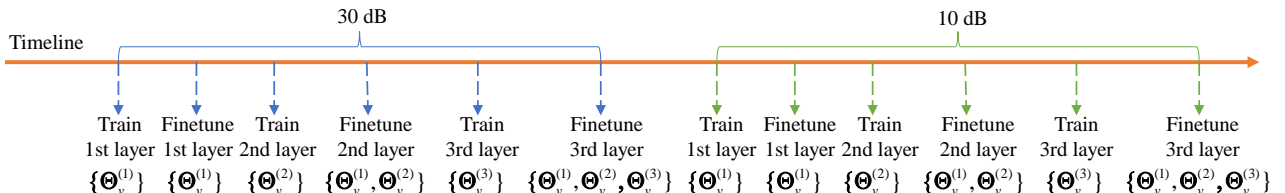


Fig. 4: Training process of a 3-layer LcgNetV (SNR = [30, 10] dB).

Furthermore, since the number of learnable parameters that are required to be optimized is limited, the training process of our proposed networks is relatively easy and simple, and it took about several hours on a standard Intel i3-6100 processor. The training time would increase with the expansion of the MIMO scale and the dimension of the learnable parameters.

E. Complexity and Memory Cost Analysis

This subsection provides the computational complexity analysis of the MMSE detector, the CG detector with L iterations, the L -layer LcgNetS and LcgNetV. The comparison is based on the number of real multiplications needed in one online detection process. In our analysis, one complex multiplication equals four real multiplications and one complex division equals four real multiplications plus one real division (RDiv).

Suppose that \mathbf{A}_{MMSE} and \mathbf{b}_{MMSE} are already calculated in advance for all the considered detectors, then the computational complexity of the MMSE detector involves: 1) the inversion of \mathbf{A}_{MMSE} , which is on the order of $\mathcal{O}(8N_t^3)$; 2) the multiplication of $\mathbf{A}_{\text{MMSE}}^{-1}$ and \mathbf{b}_{MMSE} , which requires $\mathcal{O}(4N_t^2)$ complexity. The complexity of the CG detector in each iteration includes: 1) calculating $\alpha^{(i)}$ and $\beta^{(i)}$ in (12) and (13), whose complexities can be expressed as $\mathcal{O}(4N_t^2 + 4N_t + 4) + 1$ RDiv and $\mathcal{O}(4N_t + 4) + 1$ RDiv, respectively; 2) updating $\{\hat{\mathbf{s}}^{(i)}, \mathbf{d}^{(i)}, \mathbf{r}^{(i)}\}$, which requires a complexity of $\mathcal{O}(4N_t^2 + 6N_t)$. The LcgNetS and LcgNetV exhibit the same computational complexity, which can be easily obtained by removing the calculations of $\alpha_r^{(i)}$ and $\beta_r^{(i)}$ in the CG detector. See TABLE I for a summary.

Furthermore, we investigate the memory costs of the CG detector, LcgNetS and LcgNetV, where we assume that B bits are required to store one real number. For the CG detector, only $\hat{\mathbf{s}}^{(i)}, \mathbf{d}^{(i)}, \mathbf{r}^{(i)}$ and \mathbf{A}_{MMSE} are needed to be stored for the next iteration, whose memory cost is $(6N_t + 4N_t^2)B$ bits. In the online detection process of the proposed networks, other than $\hat{\mathbf{s}}_{rm}^{(i)}, \mathbf{d}_{rm}^{(i)}, \mathbf{r}_{rm}^{(i)}$ and \mathbf{A}_{rm} , the step-sizes Θ and Θ_v are additional parameters that are required to be prestored in LcgNetS and LcgNetV, thus their memory cost can be expressed as $(6N_t + 4N_t^2 + 4L)B$ bits and $(6N_t + 4N_t^2 + 4LN_t)B$ bits, respectively.

IV. THE PROPOSED QUANTIZED LCGNETV

In the previous section, we can see that the advantage of the CG detector is its low memory costs, i.e., only $\hat{\mathbf{s}}^{(i)}, \mathbf{d}^{(i)}, \mathbf{r}^{(i)}$ and \mathbf{A}_{MMSE} are needed to be stored for the next iteration. Nevertheless, in our proposed LcgNet, we need to store all the

step-sizes (scalar step-sizes Θ in LcgNetS and vector step-sizes Θ_v in LcgNetV) since they are fixed for all problem instances. In order to reduce this memory cost, in this section, we further present a novel QLcgNetV, which is based on a specially designed soft staircase function with adjustable parameters. In the following, we will first introduce the conventional hard quantizer, and then by combining the trained LcgNetV and the proposed soft staircase function, we present the QLcgNetV, where these two important components are jointly trained. By properly optimizing the learnable parameters in the proposed soft staircase function, nonuniform quantization can be achieved with higher compression efficiency.

A. Hard Quantizer

A quantizer can be seen as a real-valued function $Q(x)$ which maps $x \in \mathbb{R}$ to a finite set $\mathcal{G} \subset \mathbb{R}$. For a vector \mathbf{x} , we define $Q(\mathbf{x}) \triangleq (Q(x_1), Q(x_2), \dots, Q(x_n))^T$. The staircase function is one of the most commonly used quantizers (also referred to as the hard quantization function), which can be expressed as

$$Q_h(x) = \begin{cases} \text{sgn}(x)G_t, & \text{if } T_t < x \leq T_{t+1} \\ 0, & \text{if } |x| \leq T_1 \end{cases}, \quad (19)$$

where $G_t \in \mathbb{R}^+$ is from a finite alphabet $\mathcal{G} = \{-G_l, \dots, -G_1, 0, G_1, \dots, G_l\}$ which consists of $2l + 1$ quantization levels and needs $\lceil \log_2(2l+1) \rceil$ bits. The elements in \mathcal{G} satisfies $G_{t_1} \leq G_{t_2}$ for any $t_1 \leq t_2$. T_t is a threshold from the set $\mathcal{T} = \{T_t \in \mathbb{R}^+ : 1 \leq t \leq l + 1\}$, and T_t is defined as

$$T_t = \begin{cases} \frac{1}{2}G_1, & \text{if } t = 1 \\ \frac{1}{2}(G_{t-1} + G_t), & \text{if } 2 \leq t \leq l \\ \infty, & \text{if } t = l + 1 \end{cases}. \quad (20)$$

The thresholds of $Q_h(x)$ are usually set as

$$\begin{aligned} \mathcal{T} &= \{-T_{l+1}, -T_l, \dots, -T_1, T_1, \dots, T_l, T_{l+1}\} \\ &= \{-\infty, -lG + \frac{1}{2}G, \dots, -\frac{1}{2}G, \frac{1}{2}G, \dots, lG - \frac{1}{2}G, \infty\}, \end{aligned} \quad (21)$$

where G is the step length between two adjacent thresholds, $lG - \frac{1}{2}G$ and $-lG + \frac{1}{2}G$ denote the upper and lower bounds, which are referred to as G_b and $-G_b$ in the following for convenience.

B. Soft Quantizer

Due to the various distributions of the network parameters, using a hard quantization function with uniformly distributed thresholds usually result in unexpected performance

TABLE I: Complexity analysis of the considered detectors

The MMSE detector		The CG detector		LcgNet	
Calculating $\mathbf{A}_{\text{MMSE}}^{-1}$	$\mathcal{O}(8N_t^3)$	Updating $\alpha^{(i)}$	$\mathcal{O}(4N_t^2 + 4N_t + 4) + 1$ RDiv		
Calculating $\mathbf{A}_{\text{MMSE}}^{-1} \times \mathbf{b}_{\text{MMSE}}$	$\mathcal{O}(4N_t^2)$	Updating $\beta^{(i)}$	$\mathcal{O}(4N_t + 4) + 1$ RDiv		
		Updating $\hat{\mathbf{s}}^{(i)}$	$\mathcal{O}(2N_t)$	Updating $\hat{\mathbf{s}}^{(i)}$	$\mathcal{O}(2N_t)$
		Updating $\mathbf{r}^{(i)}$	$\mathcal{O}(4N_t^2 + 2N_t)$	Updating $\mathbf{r}^{(i)}$	$\mathcal{O}(4N_t^2 + 2N_t)$
		Updating $\mathbf{d}^{(i)}$	$\mathcal{O}(2N_t)$	Updating $\mathbf{d}^{(i)}$	$\mathcal{O}(2N_t)$
$\mathcal{O}(8N_t^3 + 4N_t^2)$		$\mathcal{O}(L(8N_t^2 + 14N_t + 8)) + 2L$ RDiv		$\mathcal{O}(L(4N_t^2 + 6N_t))$	

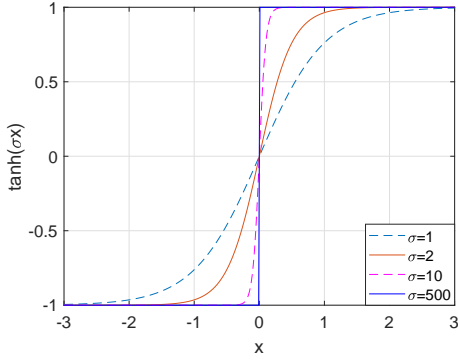


Fig. 5: The tanh function with different smoothing coefficients σ . losses [32]. Therefore, in this subsection, we aim to design an adaptive soft staircase function which is able to minimize the MSE loss function with quantized parameters, i.e. $\mathcal{L}(\{Q(\Theta^{(1)}), \dots, Q(\Theta^{(L)})\})$. Note that the hard staircase function (19) is not differentiable at the threshold points and its derivative is zero almost everywhere, this hinders the backpropagation process of the gradients. In order to overcome this difficulty and integrate an adaptive quantizer into LcgNetV directly, we propose a new soft staircase function $Q_s(\cdot)$ to approximate (19) with non-zero derivatives everywhere. The basic component of $Q_s(\cdot)$ is the following tanh(\cdot) function:

$$\tanh(x) = \frac{e^x - e^{-x}}{e^x + e^{-x}}, \quad (22)$$

which is a well-known activation function in the field of DL, and it is easy to obtain its derivatives. Fig. 5 shows the curves of $\tanh(\sigma x)$ with different values of σ , where σ can be interpreted as a smoothing coefficient. As can be seen, σ controls the degree of smoothness of $\tanh(\sigma x)$, and when $\sigma \rightarrow \infty$, $\tanh(\sigma x)$ can well approximate a hard staircase function with only one stair, i.e., the $\text{sgn}(\cdot)$ function.

Our soft staircase function, referred to as the *TanhSum* function, consists of the summation of some tanh(\cdot) functions with different offsets. Its basic form is given by

$$\text{TanhSum}(x) = \frac{G_b}{2l} \sum_{t=1}^{2l} \tanh(\sigma(x + G_b - (t-1)G)), \quad (23)$$

which contains $2l + 1$ stairs. Fig. 6 shows the curves of the proposed $\text{TanhSum}(\cdot)$ function with different values of σ for 3-bit quantization. It can be observed that similar to the tanh(\cdot) function, the $\text{TanhSum}(\cdot)$ function gradually converges to a hard staircase function with the increasing of σ . Furthermore, in order to endow the proposed $\text{TanhSum}(\cdot)$ function with the ability to learn the patterns and distributions of the network parameters, we introduce a set of learnable parameters $\Phi = \{w_{1t}, w_{2t}, b_{1t}, b_{2t}\}_1^{2l}$ to every component tanh function. As a result, we can obtain the following soft quantizer:

$$Q_s(x) = \sum_{t=1}^{2l} w_{1t} \tanh(\sigma(w_{2t}x + G_b - (t-1)G + b_{1t})) + b_{2t}, \quad (24)$$

where w_{1t} and w_{2t} are employed to adjust the length and height of the t -th level, b_{1t} and b_{2t} are the corresponding biases. From (24), we can see that the entire input-output relationship of the proposed soft quantizer can be denoted by

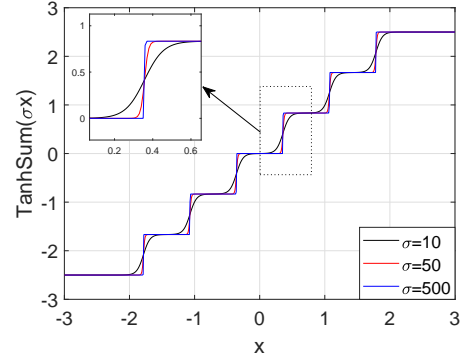


Fig. 6: The 3-bit quantization TanhSum functions with different smoothing coefficients σ .

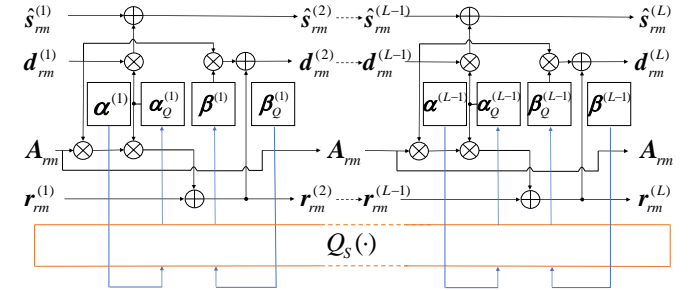


Fig. 7: The i -th layer of QLcgNetV with the proposed learnable soft quantizer.

$Q_s(\cdot; \Phi, \{\sigma, l, G_b\})$, where $\{\sigma, l, G_b\}$ represent tunable hyper-parameters which reflect the basic structure of the proposed soft quantizer.

The structure of the proposed QLcgNetV is shown in Fig. 7, where we integrate $Q_s(\cdot; \Phi, \{\sigma, l, G_b\})$ into the L -layer LcgNetV and use it to quantize the trained parameters Θ_v . It is important to note that there is only one quantizer $Q_s(\cdot)$ in the entire system, and it is used to quantize all the parameters. With given step-size parameters Θ_v , Φ are optimized by minimizing the MSE loss $\mathcal{L}_{Q_s}^{(L)}(\Phi)$ from Eq. (25) with the “annealing strategy”, i.e., we gradually increase the smoothing coefficient σ to finetune Φ and eventually the soft staircase function will converge to a discrete-valued staircase function.

V. NUMERICAL RESULTS

In this section, we first evaluate the convergence property of the proposed networks. Then, the BER performance of LcgNetS and LcgNetV is presented under both independent Rayleigh and correlated MIMO channels to demonstrate their advantages. Finally, we provide the performance of QLcgNetV to show its advantages over that with a hard quantizer. In all our simulations, the definitions of NMSE and SNR are given by

$$\text{NMSE} = E \left\{ \frac{\|\hat{s} - s\|^2}{\|s\|^2} \right\}, \quad (26)$$

$$\text{SNR} = \frac{\mathbb{E}\{\|s\|^2\}}{\mathbb{E}\{\|n\|^2\}}. \quad (27)$$

A. Convergence Property

In Fig. 8 and Fig. 9, we investigate the performance of the proposed networks with different numbers of layers or

$$\mathcal{L}_{Q_s}^{(L)}(\Phi) \triangleq \frac{1}{M} \sum_{m=1}^M \|\mathbf{s}_{rm} - \hat{\mathbf{s}}_r^{(L)}(\mathbf{y}_{rm}; Q_s(\Theta_v^{(1)}; \Phi, \{\sigma, l, G_b\}), \dots, Q_s(\Theta_v^{(L)}; \Phi, \{\sigma, l, G_b\}))\|^2 \quad (25)$$

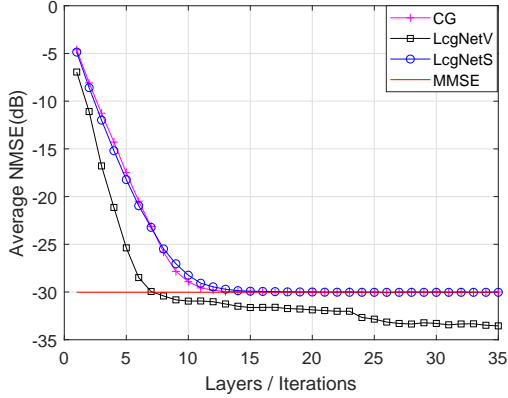


Fig. 8: NMSE versus the number of layers or iterations with SNR = 30 dB.

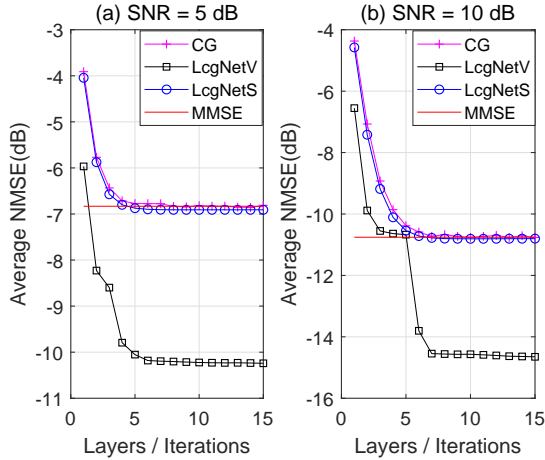


Fig. 9: NMSE versus the number of layers or iterations with SNR=5 dB and 10 dB.

equivalently iterations, in terms of NMSE. We consider a 32×64 MIMO system with Rayleigh fading channel, where each element of the channel matrix \mathbf{H} follows from a zero-mean Gaussian distribution with variance $1/N_t$. It can be observed that the convergence speed of LcgNetS is similar to that of the CG detector, while LcgNetV with high dimensional step-sizes converges much faster than those two for various SNR levels. For example, LcgNetV takes 7 layers to achieve -30 dB NMSE when SNR = 30 dB, while LcgNetS and the CG detector require 14 layers/iterations. Furthermore, LcgNetV achieves a lower NMSE than LcgNetS and the CG detector with the same L , e.g., from Fig. 8, we can see that a 6.72 dB NMSE gain can be achieved when $L = 7$. Surprisingly, it can also be seen that the performance of LcgNetV with a few layers even exceeds that of the MMSE detector (known as the performance limit of the CG detector). As shown in Fig. 9, when $L = 6$, LcgNetV achieves 3.35 dB and 3.08 dB performance gains over the MMSE detector under SNR = 5 dB and 10 dB, respectively. It can also be observed from these

two figures that in order to achieve the same performance with the MMSE detector, more layers/iterations are needed with the increasing of SNR.

B. BER Performance

In this subsection, we first provide a BER performance comparison between LcgNetV, the ML detector and the MMSE detector in Fig. 10. Due to the limitation of computing power, we only consider a 10×10 MIMO system with Rayleigh fading channel. As can be seen, although the proposed LcgNetV outperforms the MMSE detector greatly, there is still some gap to the optimal ML bound. This is mainly due to the fact that the proposed LcgNetV and the MMSE detector are both linear detectors, and their performance is known to be limited for small scale MIMO systems. Therefore, by introducing a certain level of nonlinearity into LcgNetV, its performance may be further improved, which is left for future work.

Secondly, we investigate the BER performance of the proposed networks in large scale Rayleigh fading channels, where a clear channel-hardening phenomenon can be observed. Specifically, in Fig. 11, we compare the BER performance of the proposed LcgNetS and LcgNetV with various existing MIMO detectors such as ZF, MMSE, CG and SDR [4], and three different system configurations are considered, i.e., $(N_t, N_r) = (32, 32), (32, 64), (32, 128)$. The number of layers in the proposed networks is set to be 15, and the iteration number of CG is fixed to 32. From Fig. 11, we can see that LcgNetS achieves the same performance as MMSE, and LcgNetV outperforms all the other detectors significantly in all three cases. Due to the advantages brought up by the channel-hardening phenomenon, the BER performance of all the considered detectors improves as the size of \mathbf{H} increases. If we focus on the required SNR levels to reach $\text{BER}=10^{-4}$, the performance of LcgNetV improves about 0.38 dB and 1.52 dB in the 32×64 and 32×128 massive MIMO systems than that in the 32×32 system. Furthermore, the performance improvement achieved by linear detectors, such as ZF and MMSE, is more significant than that by nonlinear detectors, e.g., SDR. For instance, in the 32×32 system, the performance of ZF is inferior to that of the SDR detector, however in the 32×64 system, ZF achieves a lower BER than SDR when $\text{SNR} > 6$ dB, and in the 32×128 system, ZF outperforms SDR for all the considered SNRs.

Finally, we investigate the BER performance of the aforementioned detectors in a spatial correlated channel model, which is known to be difficult for signal detection [33]. The numbers of antennas at the transmitter and receiver are set to $(N_t, N_r) = (32, 64)$. In this case, the channel matrix can be written in the following kronecker product form:

$$\mathbf{H} = \mathbf{R}_r^{1/2} \mathbf{U} \mathbf{R}_t^{1/2}, \quad (28)$$

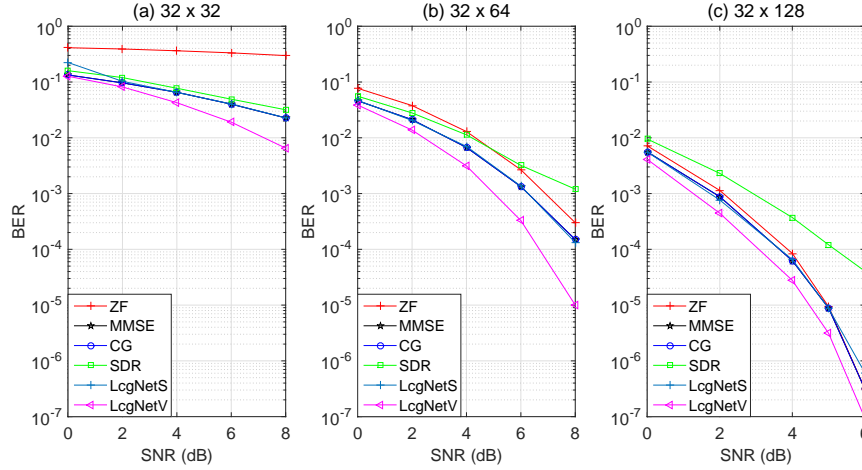


Fig. 11: BER performance comparison between the considered detectors.

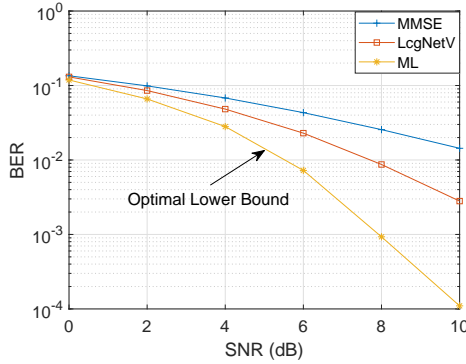


Fig. 10: BER performance comparison between LcgNetV, the MMSE detector and the ML detector in a 10×10 MIMO system.

where $\mathbf{U} \in \mathbb{C}^{N_r \times N_t}$ obeys Rayleigh distribution, $\mathbf{R}_r \in \mathbb{C}^{N_r \times N_r}$ and $\mathbf{R}_t \in \mathbb{C}^{N_t \times N_t}$ denote the spatial correlation matrices at the receiver and transmitter, respectively. \mathbf{R}_t and \mathbf{R}_r are generated from the exponential correlation model [33], whose component r_{ij} can be written as

$$r_{ij} = \begin{cases} r^{j-i}, & \text{if } i \leq j \\ r_{ji}^*, & \text{if } i > j \end{cases}, \quad (29)$$

where $|r| \leq 1$ is the correlation coefficient of neighboring receive branches and it is set to be 0.5 in this work. Fig. 12 shows the amplitudes of $\mathbf{H}^H \mathbf{H}$ in the correlated and Rayleigh channel models and it can be seen that the spatial correlation property undermines the channel-hardening phenomenon introduced by large scale antennas. Compared with the Rayleigh channel model, the matrix $\mathbf{H}^H \mathbf{H}$ in correlated channel model has smaller diagonal elements and larger off-diagonal ones, and its average amplitude difference between diagonal and off-diagonal elements is much smaller.

In Fig. 13, we present the BER performance of the considered detectors in the aforementioned correlated channel model. We can observe that in this case, all detectors experience a certain degree of performance degradation. Specifically, when we focus on the required SNR level to reach $\text{BER} = 10^{-3}$, LcgNetV and the MMSE detector exhibit about 3.12 dB and 3.63 dB performance loss due to channel correlation. However, our LcgNetV still achieves the best performance among all the

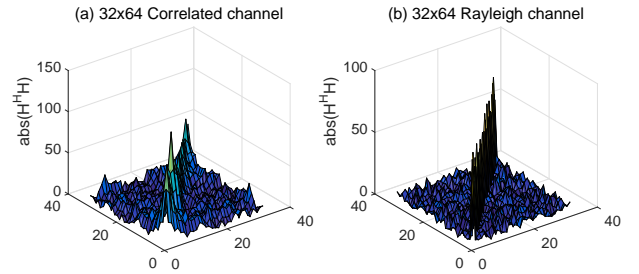


Fig. 12: An illustration of the differences between the exponential correlated and Rayleigh channel models.

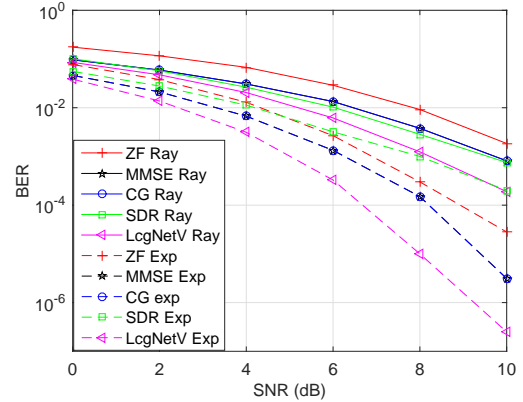


Fig. 13: BER performance comparison of the considered detectors in different channel models where *Ray* denotes the Rayleigh channel model and *Exp* represents exponential correlated channel model.

considered counterparts.

C. The Performance of QLcgNetV

We then investigate the effects of the proposed soft quantizer on LcgNetV, i.e., the performance of QLcgNetV, in a 32×64 Rayleigh fading channel. The BER performance of QLcgNetV with both hard and soft quantizers are investigated, and the number of quantization bits are chosen as 3 and 4. Given the prior knowledge of G_b obtained by LcgNetV and the required number of quantization levels, we complete the training process of QLcgNetV in three steps and the smoothing

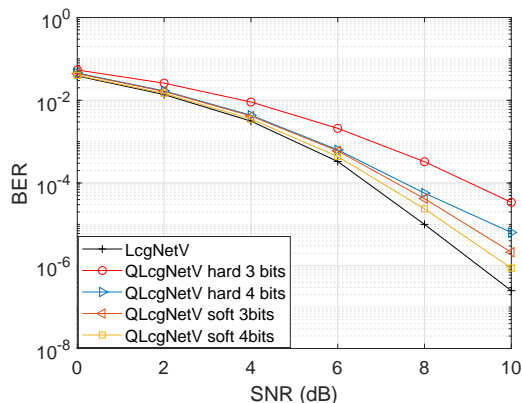


Fig. 14: BER performance comparison between LcgNetV and QLcgNetV with hard and soft quantizers.

coefficient σ used in each step is from the set $\{10, 50, 100\}$ in an increasing manner. In each training step, the learning rate is chosen from $\{1e^{-4}, 5e^{-5}, 1e^{-5}\}$ successively and the training is terminated when the average NMSE stops decreasing. The adjustable parameters $\{w_{1t}, w_{2t}, b_{1t}, b_{2t}\}$ in (24) are initialized to $\{1, 1, 0, 0\}$ and the training data set contains 10^4 samples.

As shown in Fig. 14, QLcgNetV significantly outperforms LcgNetV with a conventional hard quantizer and the BER performance achieved by a 3-bit soft quantizer is even lower than that achieved by a 4-bit hard quantizer. The performance of QLcgNetV with 3-bit and 4-bit soft quantizers is only 0.55 dB and 0.27 dB away from that without quantization at BER= 10^{-4} . This indicates that the network parameters in LcgNetV can be effectively compressed with minor performance loss. Specifically, if we assume that 32 bits are needed to store one real number without quantization and the number of layers is 15, then the memory cost of LcgNetV for storing the network parameters can be reduced from 61440 bits to 5760 bits if we employ QLcgNetV with a 3-bit soft quantizer. Also, it can be seen that there is a tradeoff between BER performance and memory cost, which mainly depends on system performance requirements and implementation.

Fig. 15 (a) and (b) depicts the staircase functions obtained by the 3-bits/4-bits hard and soft quantizers. From these two subfigures, we can see that the staircase function corresponds to the learned soft quantizer is nonuniform and its length and height are trained to fit the unquantized parameters Θ_v . Besides, we can observe that when the number of quantization bits is 4, some stairs are automatically merged into a single one and some are broken down into multiple stairs. It seems that the proposed QLcgNetV is trying to distinguish and recognize the importance of each network parameter. Also, compared with the hard quantizer, the number of stairs are reduced from 15 to 12 in this case, which shows the efficiency of the proposed quantizer.

VI. CONCLUSION

In this paper, we proposed a novel model-driven DL network structure, i.e., LcgNet, to address the fundamental massive MIMO detection problem. LcgNet is essentially designed by unfolding the iterations of the CG detector, where the

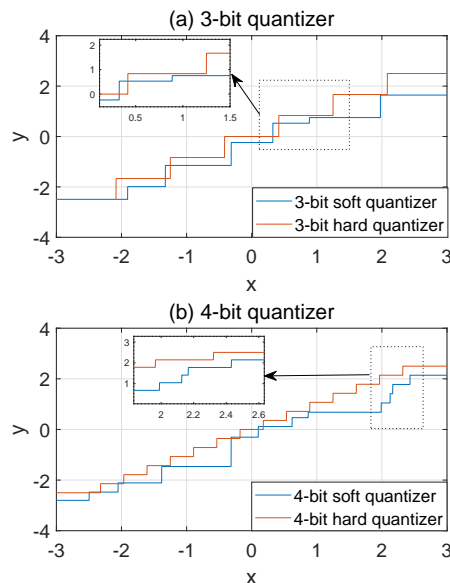


Fig. 15: Comparison of hard and soft quantizers with different numbers of bits.

differences lie in the step-sizes which are discovered to be universal and can be learned through offline training. The dimensions of the step-sizes can be augmented to further improve the detection performance. Moreover, since only a few learnable parameters are required to be optimized, the proposed networks are easy and fast to train. By inheriting the power of the CG detector and DL, the proposed network showed significant performance gain over the MMSE detector with much lower computational complexity and this performance gain is achievable under various channel models.

In addition, we presented a novel quantized LcgNetV, i.e., QLcgNetV, where a low-resolution nonuniform quantizer is integrated into LcgNetV to smartly quantize the step-sizes therein. The quantizer was designed by introducing some learnable parameters to a specially designed soft staircase function. Simulation results showed that QLcgNetV can effectively reduce the memory costs with minor detection performance loss.

VII. EXTENSIONS

In this section, we will reveal more potential applications of our proposed LcgNet and present some possible directions for future research.

Note that the CG algorithm is one of the most widely-used optimization algorithms in many practical applications. Besides the massive MIMO detection problem, the proposed LcgNet can also be employed to address many other problems, e.g., low-PAPR precoding design for massive multiuser MIMO systems [34] and robust adaptive beamforming for MIMO systems [35], etc.

This work can be viewed as an initial attempt to construct a model-driven DL network by unfolding the CG algorithm, and we validated that the performance of CG can be further improved by combining state-of-the-art DL methods. There are many interesting directions to pursue based on this idea.

For instance, some variants of the CG algorithm may also be improved by transforming their iterations into data flow graphs and training the resulting unfolded DNNs with a large number of training data, e.g., the biconjugate gradient method (BiCG) [36], the preconditioned CG algorithm for solving singular systems [37], projected CG for interior method [38], some nonlinear CG algorithms such as the Polak-Ribire-Polyak (PRP) CG algorithm [39] and the Dai-Yuan CG algorithms [40], etc.

VIII. ACKNOWLEDGEMENTS

The authors would like to thank Dr. Mingyi Hong from University of Minnesota for his valuable suggestions and criticism which improve the quality of this work.

REFERENCES

- [1] F. Rusek, D. Persson, B. K. Lau, E. G. Larsson, T. L. Marzetta, O. Edfors, and F. Tufvesson, "Scaling up MIMO: Opportunities and challenges with very large arrays," *IEEE Signal Process. Mag.*, vol. 30, no. 1, pp. 40–60, Jan. 2013.
- [2] E. G. Larsson, O. Edfors, F. Tufvesson, and T. L. Marzetta, "Massive MIMO for next generation wireless systems," *IEEE Commun. Mag.*, vol. 52, no. 2, pp. 186–195, Feb. 2014.
- [3] C. Jeon, R. Ghods, A. Maleki, and C. Studer, "Optimality of large MIMO detection via approximate message passing," in *IEEE ISIT*, Jun. 2015, pp. 1227–1231.
- [4] J. Jalden and B. Ottersten, "The diversity order of the semidefinite relaxation detector," *IEEE Trans. Inf. Theory*, vol. 54, no. 4, pp. 1406–1422, Apr. 2008.
- [5] Z. Luo, W. Ma, A. M. So, Y. Ye, and S. Zhang, "Semidefinite relaxation of quadratic optimization problems," *IEEE Signal Process. Mag.*, vol. 27, no. 3, pp. 20–34, May 2010.
- [6] T. L. Marzetta, "Noncooperative cellular wireless with unlimited numbers of base station antennas," *IEEE Trans. Wireless Commun.*, vol. 9, no. 11, pp. 3590–3600, Nov. 2010.
- [7] S. Yang and L. Hanzo, "Fifty years of MIMO detection: The road to large-scale MIMOs," *IEEE Commun. Surveys Tut.*, vol. 17, no. 4, pp. 1941–1988, 2015.
- [8] M. Wu, B. Yin, A. Vosoughi, C. Studer, J. R. Cavallaro, and C. Dick, "Approximate matrix inversion for high-throughput data detection in the large-scale MIMO uplink," in *ISCCAS*, May 2013, pp. 2155–2158.
- [9] B. Kang, J. Yoon, and J. Park, "Low complexity massive MIMO detection architecture based on neumann method," in *ISOC*, Nov. 2015, pp. 293–294.
- [10] M. Wu, B. Yin, G. Wang, C. Dick, J. R. Cavallaro, and C. Studer, "Large-scale MIMO detection for 3GPP LTE: Algorithms and FPGA implementations," *IEEE J. Sel. Topics. Signal Process.*, vol. 8, no. 5, pp. 916–929, Oct. 2014.
- [11] B. Yin, M. Wu, J. R. Cavallaro, and C. Studer, "Conjugate gradient-based soft-output detection and precoding in massive MIMO systems," in *IEEE GlobeCom*, Dec. 2014, pp. 3696–3701.
- [12] Y. Hu, Z. Wang, X. Gaol, and J. Ning, "Low-complexity signal detection using CG method for uplink large-scale MIMO systems," in *IEEE ICCS*, Nov. 2014, pp. 477–481.
- [13] Y. Xue, C. Zhang, S. Zhang, and X. You, "A fast-convergent preconditioned conjugate gradient detection for massive MIMO uplink," in *IEEE International Conference on DSP*, Oct. 2016, pp. 331–335.
- [14] S. Dörner, S. Cammerer, J. Hoydis, and S. T. Brink, "Deep learning based communication over the air," *IEEE J. Sel. Topics in Signal Process.*, vol. 12, no. 1, pp. 132–143, Feb. 2018.
- [15] T. Gruber, S. Cammerer, J. Hoydis, and S. t. Brink, "On deep learning-based channel decoding," in *51st Annual CISS*, Mar. 2017, pp. 1–6.
- [16] H. Ye, G. Y. Li, and B. Juang, "Power of deep learning for channel estimation and signal detection in OFDM systems," *IEEE Wireless Commun. Lett.*, vol. 7, no. 1, pp. 114–117, Feb. 2018.
- [17] Y. Wu, X. Li, and J. Fang, "A deep learning approach for modulation recognition via exploiting temporal correlations," in *IEEE SPAWC*, Jun. 2018, pp. 1–5.
- [18] C. Wen, W. Shih, and S. Jin, "Deep learning for massive MIMO CSI feedback," *IEEE Wireless Commun. Lett.*, vol. 7, no. 5, pp. 748–751, Oct. 2018.
- [19] Y. Wei, M. M. Zhao, M. J. Zhao, M. Lei, and Q. Yu, "An AMP-based network with deep residual learning for mmwave beamspace channel estimation," *IEEE Wireless Commun. Lett. (Early Access)*, pp. 1–1, 2019.
- [20] A. Felix, S. Cammerer, S. Dörner, J. Hoydis, and S. Ten Brink, "OFDM-Autoencoder for end-to-end learning of communications systems," in *IEEE SPAWC*, Jun. 2018, pp. 1–5.
- [21] M. Borgerdig, P. Schniter, and S. Rangan, "AMP-Inspired deep networks for sparse linear inverse problems," *IEEE Trans. Signal Process.*, vol. 65, no. 16, pp. 4293–4308, Aug. 2017.
- [22] U. S. Kamilov and H. Mansour, "Learning optimal nonlinearities for iterative thresholding algorithms," *IEEE Signal Process. Lett.*, vol. 23, no. 5, pp. 747–751, May 2016.
- [23] N. Samuel, T. Diskin, and A. Wiesel, "Learning to detect," *IEEE Trans. Signal Process.*, vol. 67, no. 10, pp. 2554–2564, May 2019.
- [24] M. Imanishi, S. Takabe, and T. Wadayama, "Deep learning-aided iterative detector for massive overloaded MIMO channels," *arXiv: 1806.10827*, 2018.
- [25] V. Corlay, J. J. Boutros, P. Ciblat, and L. Brunel, "Multilevel MIMO detection with deep learning," *arXiv: 1812.01571*, 2018.
- [26] H. He, C. Wen, S. Jin, and G. Y. Li, "A model-driven deep learning network for MIMO detection," in *IEEE GlobalSIP*, Nov. 2018, pp. 584–588.
- [27] X. Tan, W. Xu, Y. Be'ery, Z. Zhang, X. You, and C. Zhang, "Improving massive MIMO belief propagation detector with deep neural network," *arXiv: 1804.01002*, 2018.
- [28] V. A. Marcenko and L. A. Pastur, "Distribution of eigenvalues for some sets of random matrices," *Mathemat ics of the USSR-Sbornik*, vol. 1, no. 1, pp. 507–536, 1967.
- [29] J. Nocedal and S. Wright, "Numerical optimization," *Springer*, 2006.
- [30] Y. Yang, J. Sun, H. Li, and Z. Xu, "Deep ADMM-Net for compressive sensing MRI," in *NIPS*, 2016, pp. 10–18.
- [31] D. P. Kingma and J. Ba, "Adam: A method for stochastic optimization," in *Proc. Internat. Conf. on Learning Repres.*, 2015.
- [32] T. Wadayama and S. Takabe, "Joint quantizer optimization based on neural quantizer for sum-product decoder," *arXiv: 1804.06002v1*, 2018.
- [33] S. L. Loyka, "Channel capacity of MIMO architecture using the exponential correlation matrix," *IEEE Commun. Lett.*, vol. 5, no. 9, pp. 369–371, Sep. 2001.
- [34] J. Chen, "Low-PAPR precoding design for massive multiuser MIMO systems via riemannian manifold optimization," *IEEE Commun. Lett.*, vol. 21, no. 4, pp. 945–948, Apr. 2017.
- [35] M. Zhang, A. Zhang, and Q. Yang, "Robust adaptive beamforming based on conjugate gradient algorithms," *IEEE Trans. Signal Process.*, vol. 64, no. 22, pp. 6046–6057, Nov. 2016.
- [36] T. K. Sarkar, "On the application of the generalized biconjugate gradient method," *J. Electromagnet. Wave*, pp. 1:223–242, 1987.
- [37] E. F. Kaasschieter, "Preconditioned conjugate gradients for solving singular systems," *J. Comput. Appl. Math.*, pp. 24:265–275, 1988.
- [38] T. Carpenter and D. Shanno, "An interior point method for quadratic programs based on conjugate projected gradients," *Comput. Optim. Appl.*, pp. 2:5–28, 1993.
- [39] L. Zhang, W. Zhou, and D. Li, "A descent modified Polak-Ribiere-Polyak conjugate gradient method and its global convergence," *IMA Journal of Numerical Analysis*, pp. 629–640, 2006.
- [40] Y. H. Dai and Y. Yuan, "A nonlinear conjugate gradient method with a strong global convergence property," *SIAM J. Optim.*, pp. 177–182, 2000.